The *R*-matrix Calculations of Orientation and Coulomb Phase Effects in Electron–Molecule (Re-)Collisions

Alex G. Harvey and Jonathan Tennyson

Abstract Electron recollision in strong laser fields is usually studied with oriented molecules. This introduces orientation effects into the recollision problem which are generally not present in usual treatments of electron–molecule collisions. In addition this collision occurs with a molecular ion which means that the dominant electron–molecule interaction is the long-range Coulomb potential, which competes asymptotically with the strong laser field. Different workers have performed treatments varying between the complete inclusion of all asymptotic Coulomb effects to their complete neglect. Three possible treatments of the Coulomb problem are explored using H_2 and CO_2 as prototypical systems. Calculations based on *R*-matrix studies of the (re-)collision, which neglect the effects of the laser field, show that inclusion of the complete Coulomb interaction leads not only to the well-known singularity problems for forward scattering but also leads to the washing out of much of the detailed, angular structure in the differential cross section of the oriented molecules.

1 Introduction

The detailed treatment of the dynamics of a molecule trapped in a strong laser field presents a number of theoretical challenges. This is particularly true when considering electron recollision as for this case it is necessary to treat effects due to the field and the physics of the recollision process itself. In the context of electron–molecule collisions, the recollision problem actually involves the ionized electron recollid-

Alex G. Harvey
Max-Born-Institute, Max-Born-Strasse 2A, 12489 Berlin, Germany, e-mail: Alex.Harvey@mbi-berlin.de

Jonathan Tennyson
Department of Physics and Astronomy, University College London, London WC1E 6BT, UK, e-mail: j.tennyson@ucl.ac.uk

A.D. Bandrauk and M. Ivanov (eds.), *Quantum Dynamic Imaging: Theoretical and Numerical Methods*, CRM Series in Mathematical Physics, DOI 10.1007/978-1-4419-9491-2_5,

ing with the residual parent ion [1]. The theoretical treatment of field-free electron molecule collisions is itself a complex problem and an active area of research.

The R-matrix method [2] has proved highly successful in treating field-free electron-molecule collisions and is particularly well-suited to treating electron collisions with molecular ions. The method has been used to study molecular photoionization problems in weak [3] and intermediate [4, 5] fields, but has so far not been adapted for the strong field problem. The treatment of recollisions with molecules in strong fields introduce a number of effects which are not present in standard scattering calculations. The one we consider here is the fact that it is usual in strong field experiments to work with oriented molecules and therefore recollision occurs against a target ion with a definite orientation. This introduces orientation effects which are routinely averaged out when considering collisions with field-free molecules which are assumed to be oriented completely randomly. In this chapter we consider how orientation effects alter the results of these calculations. This extends work reported by us previously [6]. The particular issue we discuss here is the role of the long-range Coulomb potential as felt by the (re-)scattered electron in these recollisions. Short-range potentials that decay asymptotically faster r^{-2} are easily dealt with in the context of rescattering. The situation is less straightforward for the Coulomb potential which depends on r^{-1}. In a field free collision the range of the Coulomb potential is infinite which leads to an infinite cross section in the forward direction in the asymptotic behavior of the scattering problem. Additionally the well-known Coulomb phase is introduced due to the use of Coulomb functions instead of Bessel functions to represent the radial part of the scattering wave function. This phase can have a profound influence on on the angular distribution of scattered electrons as it changes the relative phase between partial wave components of the scattered wave, leading to constructive or destructive interference. In a strong laser field the field dominates the asymptotic behavior of the scattering and the rescattering event is in any case not actually a full collision; under these circumstances the precise role of the infinity in the forward direction and the Coulomb phase needs to be explored.

All calculation presented below are performed with the R-matrix method but in fact the reorientation issues considered below are common to all electron-molecule scattering procedures. For this reason we will not present a detailed consideration of the R-matrix method and will instead direct readers to a recent review of electron-molecule scattering using the R-matrix method by one us [7].

2 General Considerations

We discuss electron (re-)collision with aligned H_2^+ and CO_2^+ for a range of energies and alignment angles. These are high symmetry systems whose neutral ground states are both of $^1\Sigma_g^+$ symmetry. It therefore worthwhile to start by considering some effects due to symmetry. In the special case where the orientation of the molecule is such that the molecular axis is perfectly aligned parallel to the laser field

polarization, dipole selection rules restrict the overall symmetry of the scattering wave function. During ionization and subsequent acceleration in the laser field absorption of laser photons can only change the inversion symmetry of the overall wavefunction; it is clear that linearly polarized light cannot change the angular momentum of a wave function around an axis collinear with itself. This means for example that in the ionization from the CO_2 $^1\Sigma_g^+$ ground state leaving the ion in its $^2\Pi_g$ groundstate the continuum electron must have π_g or π_u symmetry and must be rotating in the opposite sense to the ion in order to preserve the component (along the molecular axis) of the angular momentum of the total wavefunction. Taking a group theory perspective we see that the dipole operator has σ_u character for this alignment. For any other alignment however it also has a π_u component and so absorption of multiple photons can lead to many different symmetries. With this in in mind we restrict the symmetry of our overall scattering wavefunctions to $^1\Sigma_u^+$ and $^1\Sigma_g^+$ corresponding to absorption of an odd or even number of photons respectively during the ionization process. We do this even in the case of nonparallel alignment, with the desire to keep the model simple in the examination of Coulomb and orientation effects. Our techniques is however fully capable of calculating the other relevant symmetry components of the wavefunction. Finally it should be noted that in a real experiment perfect alignment is not achievable and further averaging over a range molecular orientations would be required.

One technical issue is that the CO_2 scattering calculations were performed using the UK R-matrix polyatomic code [8, 9], which only works in Abelian point groups. It was therefore necessary to transform our T-matrices from D_{2h} to $D_{\infty h}$ symmetry [10]. To do the transformation it was necessary to rerun the scattering calculation, so that both degenerate target ground states were calculated ($^2B_{2g}$ and $^2B_{3g}$). Furthermore, as discussed below, the lowering of the symmetry introduces a mixing of partial waves. This is particularly important for CO_2 where Σ and Δ symmetry scattering can be important.

In the remainder of this section we give a brief description of our method for introducing orientation to the UK R-matrix code. We describe the more complex case of $D_{\infty h}$ molecules, for $C_{\infty v}$ molecules we simply need to suppress the summation over gerade and ungerade symmetries, denoted ν below, and relax the parity restrictions on the initial and final electron angular momenta, denoted l_i and l_j respectively below.

We consider an incident electron with kinetic energy $E_i = \frac{1}{2}k_i^2$ and spin projection m_{s_i} on the molecular axis from a neutral N electron target molecule of electronic state ψ_i (note: both k_i and $\mathbf{r}$ are in the lab frame).

The target electronic wave function in channel i is specified by the quantum numbers $\{\Lambda_i, S_i, M_{S_i}, \nu_i\}$. Λ_i is the projection of the angular momentum on the molecular axis, S_i is the spin, M_{S_i} is the spin projection on the molecular axis, ν_i is the gerade/ungerade nature of the state and m_{s_i} is the spin projection of the incident electron. The Euler angles (α, β, γ) specify the orientation of the molecule. $\{\Lambda, S, M_S, \nu\}$ are the quantum numbers of the $N + 1$ system of the target plus the scattering electron and are invariant throughout the collision. The molecular frame T-matrix calculated by the UK R-matrix codes is related to the lab frame scattering

amplitude in the following manner [10]

$$F_{ij}(\theta,\phi;\alpha,\beta,\gamma) = f_i^C(\theta)\delta_{il_i jl_j} + \frac{\sqrt{\pi}}{\mathrm{i}\sqrt{k_i k_j}} \sum_{\substack{\Lambda S M_S v \\ \bar{l}_i \bar{l}_j m_{\bar{l}_j}}} \mathrm{i}^{\bar{l}_i - \bar{l}_j} \sqrt{2\bar{l}_i + 1}\, \mathrm{e}^{\mathrm{i}(\sigma_{l_i}+\sigma_{l_j})} \times D^{\bar{l}_j}_{m_{\bar{l}_j}\,\Lambda-\Lambda_j}(\alpha,\beta,\gamma) Y^{m_{\bar{l}_j}}_{\bar{l}_j}(\hat{r}) C_j \times T^{\Lambda S v}_{\bar{i}\bar{l}_i\,\bar{j}\bar{l}_j} C_i^* D^{\bar{l}_i *}_{0\Lambda-\Lambda_i}(\alpha,\beta,\gamma) \tag{1}$$

where the Coulomb phase is given by

$$\sigma_{l_i} = \arg\Gamma(l_i + 1 + \mathrm{i}\eta_i) \tag{2}$$

$$\eta_i = -\frac{Z-N}{k_i} \tag{3}$$

and $C_{i/j} = \langle S M_S | S_{i/j} M_{S_{i/j}} \frac{1}{2} m_{s_{i/j}} \rangle$ are Clebsch–Gordan coefficients. The differential cross section is then

$$\begin{aligned} \left.\frac{\mathrm{d}\sigma}{\mathrm{d}\Omega}\right|_{ij} &= \frac{k_j}{k_i}|F_{ij}|^2 \\ &= \frac{k_j}{k_i}\left[|f_i^C|^2\delta_{il_i jl_j} + |F_{ij}^{(\mathrm{add})}|^2 + \left[f_i^C F_{ij}^{(add)*} + f_i^{C*} F_{ij}^{(\mathrm{add})}\right]\delta_{il_i jl_j}\right] \\ &= \frac{k_j}{k_i}\left[|F_{ij}^{(\mathrm{add})}|^2 + \delta_{il_i jl_j}\left[|f_i^C|^2 + 2\,\mathrm{RE}\left[f_i^C F_{ij}^{(add)*}\right]\right]\right], \end{aligned} \tag{4}$$

where $F_{ij}^{(\mathrm{add})}$ is the second term on the right-hand side of (1). We note that $F_{ij}^{(\mathrm{add})}$ differs from the oriented scattering amplitude for a neutral molecule only in the the term $\mathrm{e}^{\mathrm{i}(\sigma_{l_i}+\sigma_{l_j})}$ involving the Coulomb phases.

Several models for calculating aligned differential cross sections are examined. The first (Model I), which has been explored by us previously [6], considers neither the pure Coulomb scattering and interference term (that exist in the elastic channel), nor the Coulomb phase in the short-range term [6]. The second (Model II), following Sheehy et al. [11] includes the Coulomb phase in the short range term but not the Coulomb scattering and interference terms. In the third model (Model III) the effects of adding the entire Coulomb scattering and interference terms are considered in full. This approach, which was used recently by Chen et al. [12], has issues with infinite cross sections for forward scattering although there do appear to be regularization procedures for treating this issue [13]. Results are presented for each of these models in the illustrative calculations presented below.

3 Results for Molecular Hydrogen

The T-matrix elements obtained previously [1] were used for all the calculations. Only the states of ${}^1\Sigma_u^+$ and ${}^1\Sigma_g^+$ symmetry are considered, which is sufficient for the case of parallel alignment.

Figure 1 shows the total cross section for electron rescattering from parallel aligned H_2 against incident electron energy using Model I. The cross sections are approximately 3–4 times greater in magnitude than the orientationally averaged case, this is what we might expect taking the simplistic view that the electron takes a longer path through the molecule and so has more opportunity to interact with it. Compared to previous, orientationally averaged calculations [1, 14], they show similar resonance structure up to the first electronic excitation threshold; however the series of Feshbach resonances converging on the second excited state are heavily suppressed.

Model I

Figure 2 shows parallel aligned differential cross sections for a range of nonresonant energies. With this alignment, due to the symmetry of the system, the differential cross section is a function of θ alone. We see that ${}^1\Sigma_g^+$ symmetry differential cross sections are markedly different in shape than the orientationally averaged case. All the differential cross sections are symmetric about 90°; this is to be expected as elastic scattering of single total symmetry will have a continuum described entirely by a sum of either gerade or ungerade spherical harmonics depending on the gerade/ungerade symmetry of the target state; these sums are symmetric around 90°. For energies below the first resonance at, 12.87 eV, we can see that the differential cross sections have strong peaks in the forward and backwards direction and slightly lower peaks at 90°. Interestingly at 15.5 eV, in between the first and second resonances, we see a significant change in shape that appears to be an inversion,

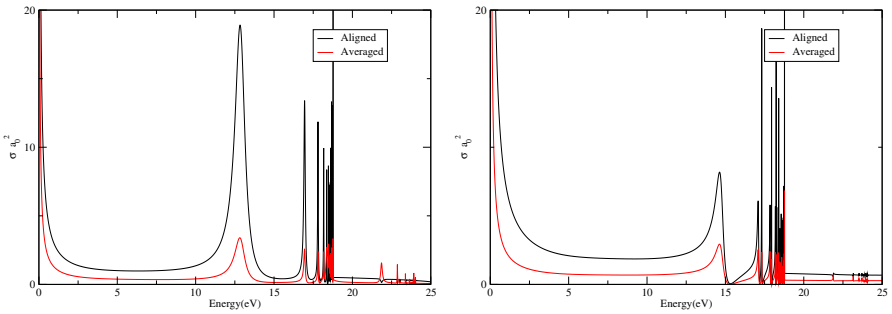

Fig. 1 Total cross section as function of energy for the parallel aligned electron–H_2^+ collision problem (Model I): left figure ${}^1\Sigma_g^+$ total symmetry, right figure ${}^1\Sigma_u^+$ symmetry.

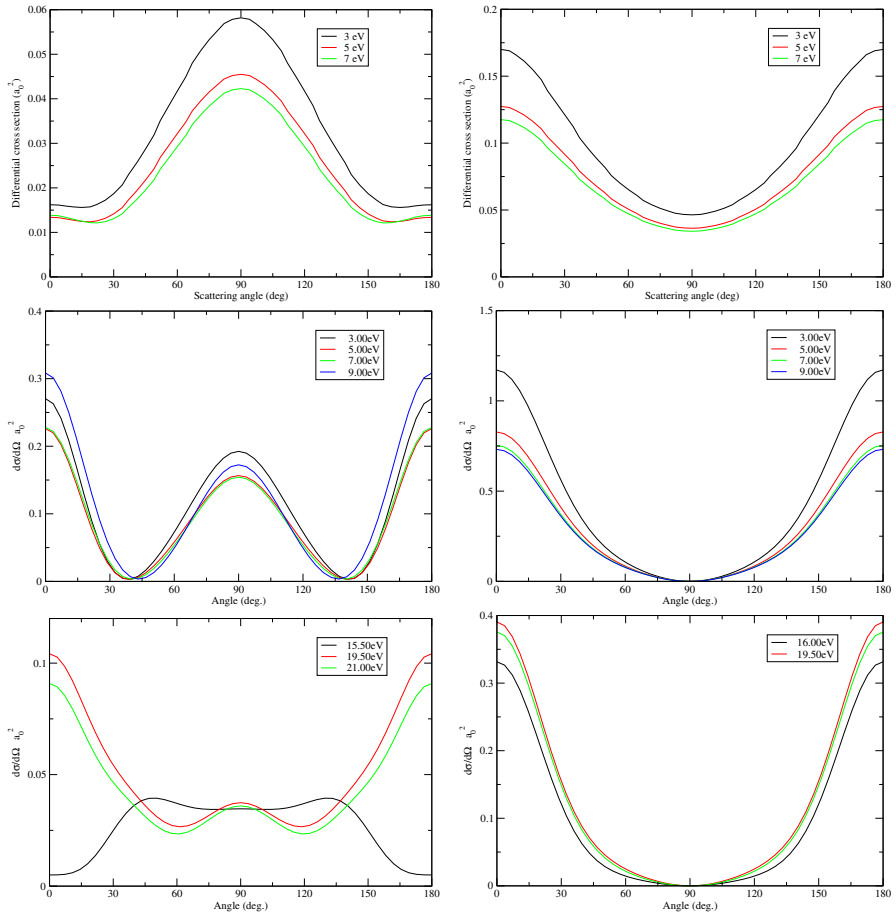

Fig. 2 Model I: Differential cross sections for parallel aligned electron–H_2^+ collisions for seven electron collision energies (Top row: orientationally averaged case): left-hand figures $^1\Sigma_g^+$ symmetry, right-hand figure $^1\Sigma_u^+$ symmetry.

with minima in the forwards and backwards direction. This may be a phase effect due to passing through the first resonance. Above the first excited state we again get strong forwards and backwards scattering, however the peak at 90° is significantly less pronounced. The $^1\Sigma_u^+$ symmetry shows strong forwards and backwards scattering, unlike $^1\Sigma_g^+$ symmetry, there is no sideways scattering and no significant shape difference between the aligned and orientationally averaged cases, or change of shape as a function of energy.

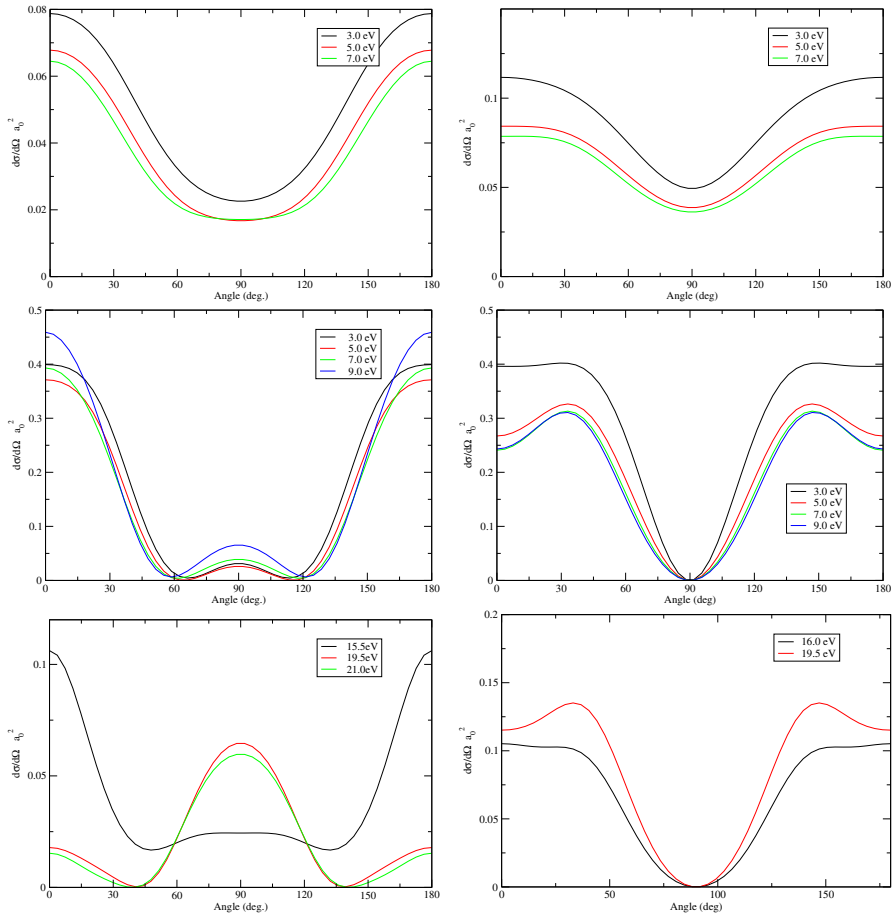

Fig. 3 Model II: Differential cross sections for parallel aligned electron–H_2^+ collisions for seven electron collision energies (Top row: orientationally averaged case): left-hand figures $^1\Sigma_g^+$ symmetry, right-hand figure $^1\Sigma_u^+$ symmetry.

Model II

Figure 3 shows the same plots as Fig.2 but now with the Coulomb phase added. We can see now that the addition make a marked qualitative difference to the differential cross section. For the $^1\Sigma_g^+$ symmetry, for energies less than 15.5 eV the phase (which has an energy dependence) tends to enhance the cross section in the forward and backwards directions and suppress scattering at 90°. The effect is extreme in the orientationally averaged case which has been almost inverted when compared to its Model I counterpart, in the parallel aligned case the central peak (at 90°) is strongly suppressed. The 19.5 eV cross section, which appeared inverted in Model I is still inverted and the central peak has been enhanced. The differential cross section at

21 eV now also appears to be inverted. This however must be due to the Coulomb phase and not from passing through a resonance as the Model I cross section is not inverted. So we can see that the addition of a Coulomb phase makes the shape of these differential cross sections strongly energy dependent, as might be expected due to the energy dependence of the Coulomb phase.

The $^1\Sigma_u^+$ symmetry for the orientationally averaged case has undergone a less dramatic transformation, with forward and backwards scattering being slightly suppressed. For the parallel aligned cases the major change is again suppression of the forward and backwards direction and the addition of a slight maximum between 30–35°, these shape appears to be stable over the energy range considered.

Model III

Addition of the Coulomb scattering and interference term, Fig. 4, largely obscures the features due to short range forces, especially for small angle scattering. This is as one might expect on the consideration that the Coulomb scattering term is significantly higher than the short range forces term across the majority of the angular range. One way to extract information from these cross sections is to normalize them to the pure Coulomb differential cross section at the same energy.

Figure 5 shows the differential cross sections normalized in this fashion, they show the proportional effect the short range force and interference terms have on the the pure Coulomb differential cross section. One common feature to all of the normalized cross sections is that the proportional deviation from Coulomb scattering is low at small angles and increases for larger angles. This is to be expected as the scattering due to short range forces does not vary greatly in magnitude over the angular range in comparison to Coulomb scattering which changes by many orders of magnitude. We also see that for large angle scattering, with $\theta > 90°$, that the angular structure seen in Model II is to a certain extent preserved.

In Fig. 6 we have plotted total cross section versus alignment angle β. We see that both the $^1\Sigma_g^+$ and $^1\Sigma_u^+$ components are strongly peaked for parallel alignment,

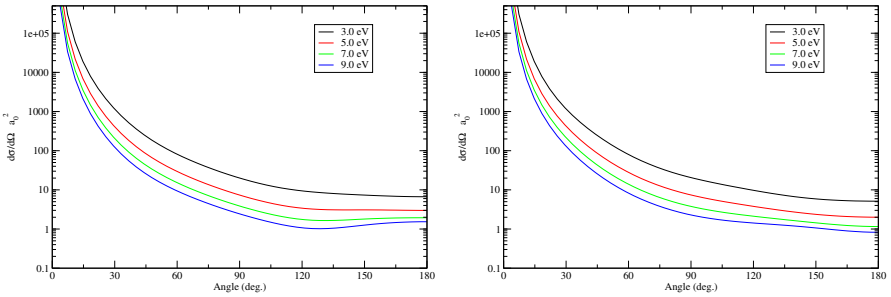

Fig. 4 Model III: Differential cross sections for parallel aligned electron–H_2^+ collisions for 4 electron collision energies: left-hand figures $^1\Sigma_g^+$ symmetry, right-hand figure $^1\Sigma_u^+$ symmetry.

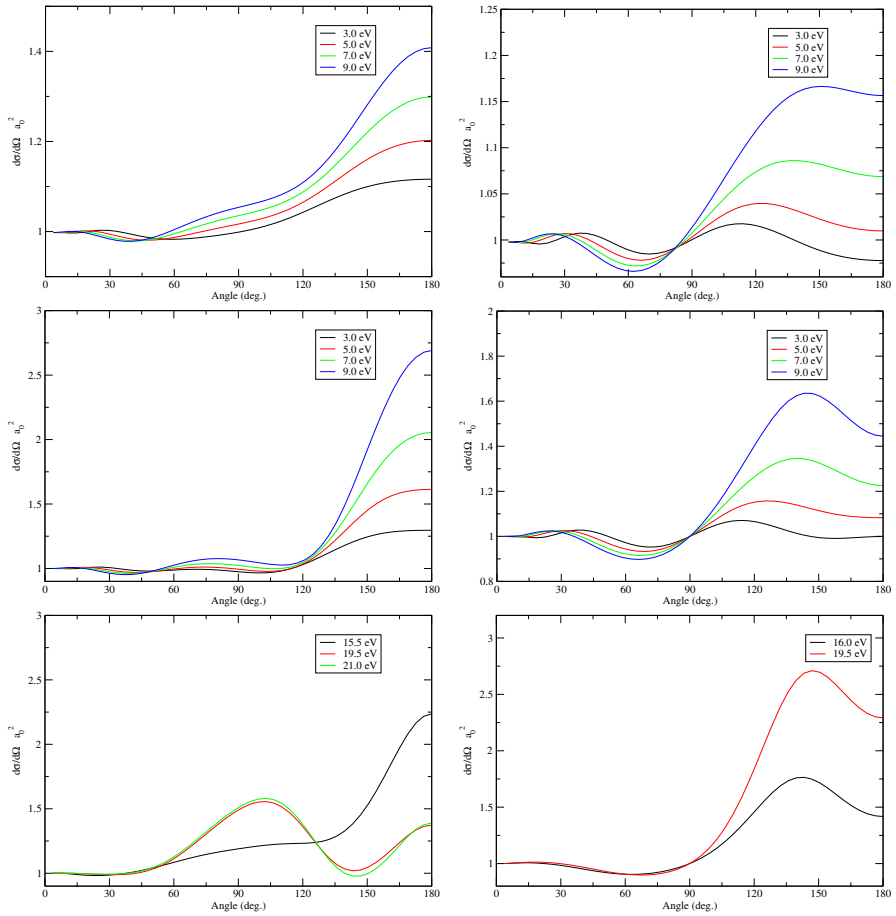

Fig. 5 Model III: Differential cross sections (normalized to pure Coulomb scattering) for parallel aligned electron–H_2^+ collisions for seven electron collision energies (Top row: orientationally averaged case): left-hand figures $^1\Sigma_g^+$ symmetry, right-hand figure $^1\Sigma_u^+$ symmetry. Dimensionless units.

with $^1\Sigma_g^+$ having an additional smaller peak at perpendicular alignment while $^1\Sigma_u^+$ is zero. Due to the $^2\Sigma_g^+$ ground state of the cation we expect the contribution of higher symmetries for nonparallel alignments to be relatively minor. These observations justify the use of parallel alignment in rescattering experiments on H_2. It is apparent that the addition of a Coulomb phase makes no difference to the integral cross section.

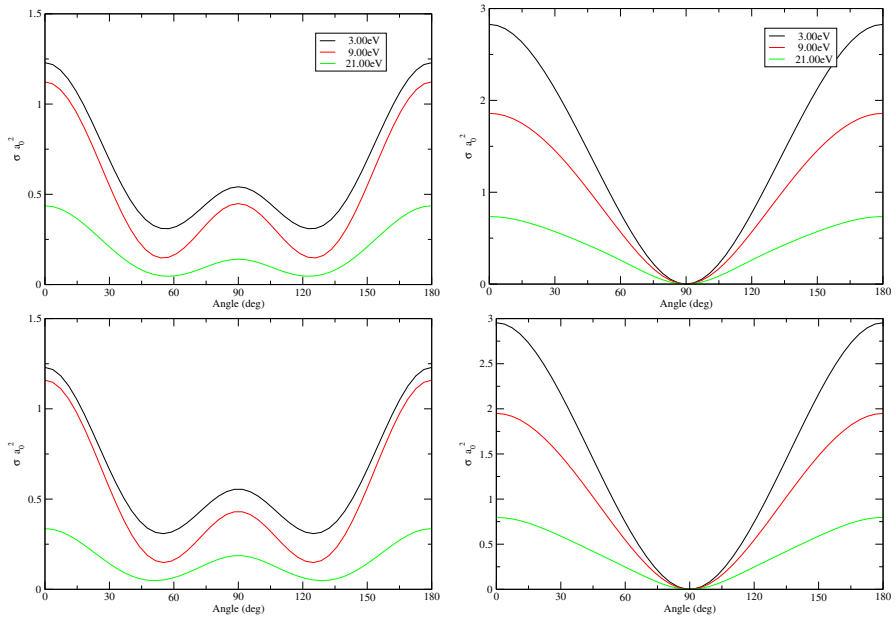

Fig. 6 Total cross section as function of alignment angle β for the aligned electron–H_2^+ collision problem at a range of energies:top figures Model I, bottom figures Model II, left figures $^1\Sigma_g^+$ total symmetry, right $^1\Sigma_u^+$ symmetry.

4 Results for Carbon Dioxide

The T-matrix elements obtained previously [1] were used for all the calculations.

Figure 7 compares the orientationally averaged $D_{\infty h}$ total cross sections (calculated in Model I) for $^1\Sigma_g^+$ and $^1\Sigma_u^+$ symmetries with the corresponding results for

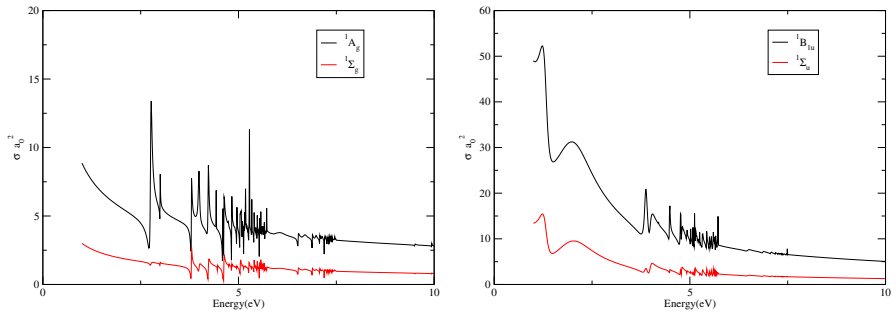

Fig. 7 Model I: Total cross section as function of energy for the orientationally averaged electron–CO_2^+ collision problem comparing original D_{2h} and transformed to $D_{\infty h}$ symmetries (Model I): left figure ^1A_g and $^1\Sigma_g^+$ total symmetry, right figure $^1B_{1u}$ and $^1\Sigma_u^+$ symmetry.

^1A_g and $^1B_{1u}$ from the original D_{2h} calculations. These are the D_{2h} symmetries which contain the $^1\Sigma^+$ contributions. We see that the ^1A_g and $^1B_{1u}$ D_{2h} symmetry cross sections are approximately three to four times larger than their respective $D_{\infty h}$ symmetry counterparts, $^1\Sigma_g^+$ and $^1\Sigma_u^+$. This is because the D_{2h} cross sections contain significant contributions from the $^1\Delta$ components. The $^2\Pi_g$ target and π continuum couple to give $^1\Sigma$ and $^1\Delta$ total symmetry and both these symmetries are contained in the corresponding D_{2h} T-matrix elements. It can be anticipated that cross sections of $^1\Pi_g$ total symmetry will be dominant at low collision energies as they couple to a σ_g continuum. It should be noted that the resonance structure is unchanged, we still see infinite series of Feshbach resonances below each threshold [1], a higher energy resolution would resolve more of these.

Figure 8 shows total cross section for $^1\Sigma^+$ symmetries as a function of the alignment angle β. We immediately see that for both symmetries we get zero total cross section for the parallel aligned case and therefore zero differential cross sections; this is a direct consequence of the $^2\Pi_g$ symmetry of the CO_2^+ target. It is important to note that, for alignments other than parallel, it is necessary to sum over higher symmetries to give the correct differential cross sections, these are expected to be significant due to the $^2\Pi_g$ ground state of the cation. We see that for the $^1\Sigma_g^+$ component the cross sections have a maxima between 50–55° and 140–145°, depending on energy, and are zero at 90° and 0°.

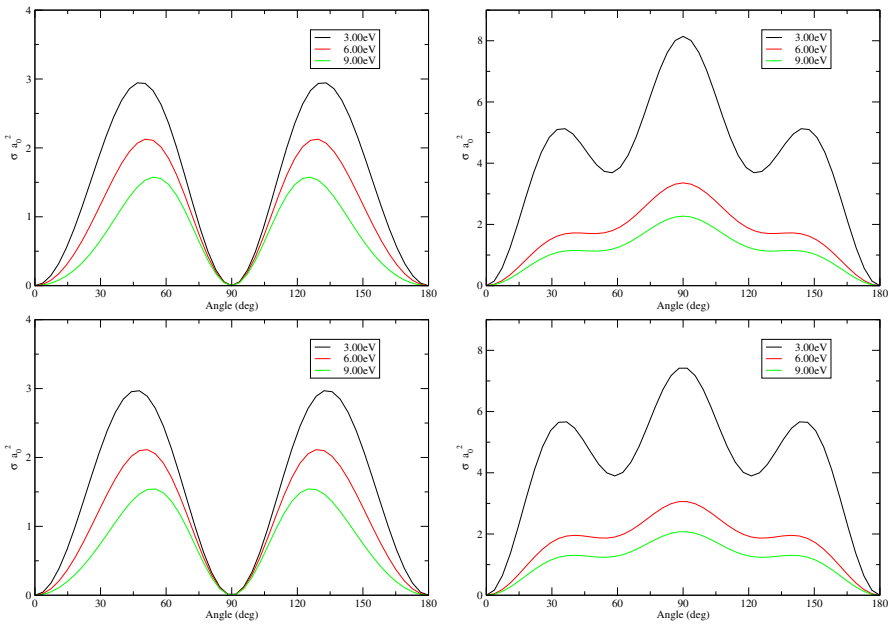

Fig. 8 Total cross section as function of alignment angle β for the aligned electron–CO_2^+ collision problem at a range of energies: Top figures Model I, Bottom Model II, left figure $^1\Sigma_g^+$ total symmetry, right $^1\Sigma_u^+$ symmetry.

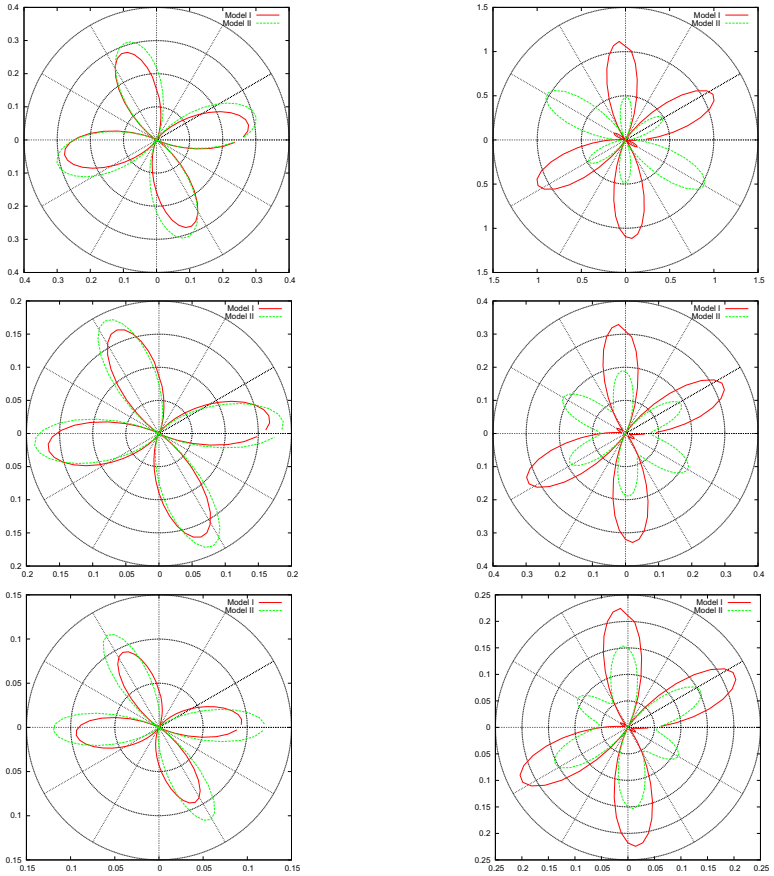

Fig. 9 Model I & Model II: Polar plots of the differential cross section taken in the zx plane with $\beta = 30°$ for the aligned electron–CO_2^+ collision problem, top row 3 eV, middle row 6 eV, bottom row 9 eV: left figures $^1\Sigma_g^+$ total symmetry, right $^1\Sigma_u^+$ symmetry. The scale is in units of a_0 and gives the r values for the circular grid.

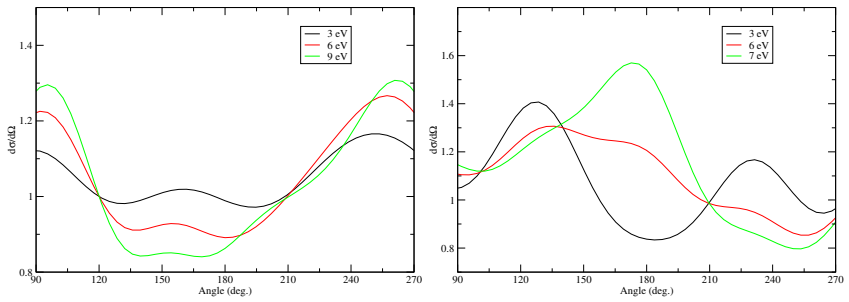

Fig. 10 Model III: Normalized differential cross section taken in the zx plane with $\beta = 30°$ for the aligned electron–CO_2^+ collision problem, backwards scattering angles only, θ measured from z-axis. Left figure $^1\Sigma_g^+$ total symmetry, right $^1\Sigma_u^+$ symmetry. Dimensionless units.

For $^1\Sigma_u^+$ there is a maximum at 90° in contrast with $^1\Sigma_g^+$, and there are smaller peaks between 35–40° and 125–130°. These observations agree with the recent study on HHG with CO_2 by Mairesse et al. [15]. Again there is no difference between Model I and Model II integral cross sections for $^1\Sigma_g^+$. However there is a slight depression of the central peak and raising of the side peaks for the $^1\Sigma_u^+$.

Model I

Figure 9 shows the $^1\Sigma^+$ part of the differential cross section given in polar coordinates with r being the magnitude of the differential cross section and θ measured from the z-axis. The differential cross sections are symmetrical around the molecular axis, this suggests that the zx plane, containing the molecule, is an appropriate plane in which to examine them. We see that for $^1\Sigma_g^+$ the differential cross section is zero parallel and perpendicular to the molecular axis. $^1\Sigma_u^+$ is also zero in the parallel direction but has a small peak perpendicular to the molecular axis and is approximately 4 times greater in magnitude than $^1\Sigma_g^+$.

Model II

The addition of the Coulomb phase makes little difference to the $^1\Sigma_g^+$ differential cross sections across the energy range studied in contrast to the H_2 case. For the $^1\Sigma_u^+$ symmetry we see a strong enhancement of scattering perpendicular to the molecular axis and a corresponding reduction in the maxima in either directions. The direction of the maxima and minima are stable across the energy range considered. Further work to extend the energy range by including more target states and using the molecular R-matrix with pseudo state method [16, 17] for energies near and above the ionisation threshold would allow us to further examine the effect of the Coulomb phase with increasing energy.

Model III

Figure 10 shows differential cross sections normalized to the Coulomb cross section, for scattering angles in the backwards direction. For this model the polar plots of the last two models have been abandoned as they would show small deviation from a unit circle. The backward direction was chosen as the deviation from Coulomb scattering is small for small angle scattering. Examining the figure we see that zero scattering due to short range forces in the direction of the molecular axis is preserved (corresponding to a value of unity) in all cases, as one would expect. For the $^1\Sigma_g^+$ the position of maxima is shifted slightly to larger scattering angles. The Model II maxima at 150° is less than unity in Model III, this is due to the relative phase of the Coulomb scattering amplitude and the amplitude due to short range forces which controls whether the interference term is additive or subtractive. Comparing

Model II to Model III for ${}^1\Sigma_u^+$ we see that the maxima are again preserved as in the ${}^1\Sigma_g^+$ case, however maxima separated by nonzero local minima become harder to resolve as the minima become much less pronounced.

5 Conclusions

Integral and differential cross sections for rescattering from parallel aligned H_2 and CO_2 are presented which consider three different models for treating the effects of the long-range Coulomb potential. In H_2 for all models, the results show that for the ${}^1\Sigma_g^+$ symmetry both integral and differential cross sections are greater in magnitude and that differential cross sections also differ in shape in comparison to the nonaligned situation. We see strong forward and backwards scattering in contrast to the minima at these direction in the unaligned case. We also see that the shape of the differential cross section can change significantly before and after a resonance. The addition of a Coulomb phase has a marked effect on the cross sections, with a tendency to enhance or suppress forwards, backwards and sideways scattering dependent on the energy, due to constructive or destructive interference between partial waves. Inclusion of the Coulomb scattering and interference terms obscures much of the angular structure seen in the differential cross sections, however through normalization to pure Coulomb scattering some of the structure can be recovered giving qualitatively similar shapes for scattering angles greater than 90°

For CO_2 we find that parallel alignment gives zero cross sections due to short range forces indicating a need to perform this type of experiment at nonparallel alignments. We also see that perpendicular alignment gives a zero cross section for ${}^1\Sigma_g^+$ and a maximum for ${}^1\Sigma_u^+$, however further work to include higher symmetries is required to gain an accurate picture of nonparallel alignments. Again examining the differential cross sections we see that the addition of the Coulomb phase has an effect of suppressing and accentuating the various maxima. In this case the strongest effect was seen for the ${}^1\Sigma_u^+$ symmetry. The ${}^1\Sigma_g^+$ symmetry showed little change with the addition of the Coulomb phase. Inclusion of the Coulomb scattering and interference terms has a greater effect in obscuring the structural information present in scattering from short range forces than in H_2.

We note that the latest models of recollision find it important to explicitly allow for electron impact electronic excitation of the target ion [18]; this process is automatically included in our scattering treatment.

This study ignores the undeniably important effect of the external laser field on the scattering electron. It is straightforward to add a weak field using our current techniques [3] but adding a strong field requires a time dependent treatment. There are two possible approaches to overcoming the omission of the laser field. One is to incorporate the laser effects within the R-matrix approach. We note that the formalism for this was given sometime ago [19] but has only recently been implemented for the atomic case [20]. Generalization of this to molecular systems would give a

consistent treatment of the problem but remains both technically and computationally challenging. Work in this direction is just commencing.

The other possibility is to incorporate our field free scattering calculation in a strong field model. The Coulomb singularity in the forward direction is a consequence of the breakdown of the validity (in the forward direction) of the asymptotic division of the scattering wavefunction into an incident and scattered wave of infinite extent. In other words the singularity is not in the scattering wave function but in the asymptotic form. Of course infinite waves of precisely defined momentum are unphysical, in strong field experiments the incoming electron wave packet has dimensions measured in tens of Bohr. This is precisely the point at which a connection to a strong field model can be made. One option is to regularize the cross section as discussed in [13], using the information about the incident wave packet from a strong field model. The R-matrix method gives us the full scattering wavefunction [7], this suggests another approach, that is to use the scattering wavefunctions to create an incident wave packet of size and shape informed by a strong field model, then calculate the flux at some appropriate distance from the molecule. This would have the benefit of allowing ideas of electron holography to be explored, which rely on the interference of incident and scattered parts of the wavepacket explicitly excluded in the standard definition of a cross section.

Acknowledgements This work was performed as part of an EPSRC funded project to study ultrafast molecular imaging. We acknowledge helpful discussions with all members of the consortium and in particular Jon Marangos, Misha Ivanov, Olga Smirnova and Jonathan Underwood.

References

1. A. Harvey, J. Tennyson, J. Mod. Opt. **54**, 1099 (2007)
2. P.G. Burke, K.A. Berrington (eds.), *Atomic and Molecular Processes, an R-matrix Approach* (IOP Pub., Bristol, 1993)
3. J. Tennyson, C.J. Noble, P.G. Burke, Int. J. Quantum Chem. **29**, 1033 (1986)
4. J. Colgan, D.H. Glass, P.B. K. Higgins, Comput. Phys. Commun. **114**, 27 (1998)
5. P.G. Burke, J. Colgan, D.H. Glass, K. Higgins, J. Phys. B **33**, 143 (2000)
6. A.G. Harvey, J. Tennyson, J. Phys. B **42**, 095101 (2009)
7. J. Tennyson, Phys. Rep. **491**, 29 (2010)
8. L.A. Morgan, J. Tennyson, C.J. Gillan, Comput. Phys. Commun. **114**, 120 (1998)
9. L.A. Morgan, C.J. Gillan, J. Tennyson, X. Chen, J. Phys. B **30**, 4087 (1997)
10. A.G. Harvey, Electron re-scattering from aligned molecules using the R-matrix method. Ph.D. thesis, University College London (2010)
11. B. Sheehy, R. Lafon, M. Widmer, B. Walker, L.F. DiMauro, P.A. Agostini, K.C. Kulander, Phys. Rev. A **58**, 3942 (1998)
12. Z. Chen, A.T. Le, T. Morishita, C.D. Lin, Phys. Rev. A **79**, 033409 (2009)
13. V.G. Baryshevskii, I.D. Feranchuk, P.B. Kats, Phys. Rev. A **70**, 052701 (2004)
14. J. Tennyson, At. Data Nucl. Data Tables **64**, 253 (1996)
15. Y. Mairesse, J. Levesque, N. Dudovich, P.B. Corkum, D.M. Villeneuve, J. Mod. Opt. **55**, 2591 (2008)
16. J.D. Gorfinkiel, J. Tennyson, J. Phys. B **37**, L343 (2004)
17. J.D. Gorfinkiel, J. Tennyson, J. Phys. B **38**, 1607 (2005)

18. S. Graefe, M.Y. Ivanov, J. Mod. Opt. **55**, 2557 (2008)
19. P.G. Burke, V.M. Burke, J. Phys. B **30**, L383 (1997)
20. H.W. van der Hart, M.A. Lysagt, P.G. Burke, Phys. Rev. A **76**, 043405 (2007)